The Astrophysical Journal, 615:286–299, 2004 November 1

OPTICAL PROPERTIES OF COMPOSITE INTERSTELLAR GRAINS: A MORPHOLOGICAL ANALYSIS

Maria Antonia Iatì,[1] Arianna Giusto,[1] Rosalba Saija,[1] Ferdinando Borghese,[1] and Paolo Denti[1]
Dipartimento di Fisica della Materia e Tecnologie Fisiche Avanzate, Università di Messina, Salita Sperone 31, 98166 Messina, Italy; iati@ortica.unime.it

Cesare Cecchi-Pestellini
Dipartimento di Fisica, Università di Lecce, Via di Arnesano, 73100 Lecce, Italy

and

Santi Aiello
Dipartimento di Astronomia e Scienza dello Spazio, Università di Firenze, Largo E. Fermi 5, 50125 Florence, Italy
Received 2004 February 13; accepted 2004 July 9

ABSTRACT

In the framework of the transition matrix approach, we calculate the relevant optical properties of cosmic dust grains of amorphous carbon and astronomical silicates, modeled as aggregates of spherical monomers. Two mechanisms of aggregation were considered, producing clusters with different structure and degree of fluffiness: ballistic particle-cluster aggregation (BPCA) and ballistic cluster-cluster aggregation (BCCA). Our results are very different from those obtained through computational approaches based on effective medium theories and might have major implications both on the modeling procedure and on the dust-mass balance in the interstellar medium.

Subject headings: astrochemistry — dust, extinction — radiative transfer

1. INTRODUCTION

Although there is little direct knowledge of the true nature of interstellar dust grains, two pieces of evidence point toward the possibility that interstellar grains are composites of many small grains of silicates and (amorphous) carbon (Mathis & Whiffen 1989). First, dust grains are thought to grow through coagulation (Jura 1980), rather than by gas accretion onto their surfaces (Draine 1985a). During the process smaller grains collide and stick together to form larger grains, with cavities and voids incorporated into the conglomerate. Second, studies of interplanetary and cometary dust indicate that cosmic grains are likely to be porous and fluffy (Krueger & Kissel 1989; Hagen & Greenberg 1990; Wolff et al. 1994). These grains appear to consist of units (monomers) whose sizes are tens of nanometers. Monomers can aggregate into fluffy particles with typical sizes 0.1–10 μm. They are made of a mineral Si- and Mg-based backbone with catalytically active metals such as Fe, Ni, Ti, Zn, Ca, and Mg. Recently, Bradley et al. (1999) have identified porous interplanetary dust particles in the matrices of chondrites. These particles are silicates embedded in a layer of amorphous carbon showing absorption features near 9 and 18 μm. They have a typical size of 0.5 μm and contain FeNi and FeSi nano-sized inclusions that are superparamagnetic, Mg-rich, and Fe-poor, and the elemental content is as predicted from depletion measurements. Such properties are very close to the ones desirable for interstellar dust. Thus, these particles may be a sample of largely unprocessed interstellar dust grains. It is well known that the extinction differs appreciably between the diffuse interstellar medium (ISM) and dense clouds. As a consequence, grain size distribution and possibly chemical composition of grains must undergo major modifications during grain lifetime as dust grains cycle through several diffuse/dense phase transitions. The formation of aggregates by coagulation has been discussed extensively (Ossenkopf 1993; Chokshi et al. 1993; Weidenschilling & Ruzmaikina 1994; Dominik & Tielens 1995, 1996). We summarize the complicated evolutionary process of the modification of grain size distribution, exploiting random single-particle aggregation and ballistic cluster-cluster aggregation (§ 2). The extent of fluffiness depends on the particular hosting region, and it is likely to be quite variable. The identification of sustainable structures for dust grains in the typical physical and chemical conditions of the diffuse ISM is related to the determination of the pattern of the elemental depletions. The point is crucial because out to 1500 pc the gas-phase abundances of C/H, O/H, and Kr/H are stable in diffuse clouds with different physical conditions as measured by the fraction of H in the form of H_2. This uniformity suggests that there is a standard local ISM abundance and that this standard must be related to the grain structure, since the extinction per unit mass depends critically on the morphology of the scatterer.

In this work, grain aggregates are assumed to be fluffily substructured collections of very small particles loosely attached to one another. Each particle is assumed to consist of a single material, such as silicates or carbon, as formed in the various separate sources of cosmic dust. To emphasize the different roles of morphology and chemical composition, we consider both homogeneous and inhomogeneous grain aggregates. Voids are naturally generated by random accretion of particles leading to cavities of sizes comparable to those of the coagulating grains. Because of the complexity in morphology and composition, the optical properties of these irregularly shaped aggregates are quite different from those of solid homogeneous spheres (Saija et al. 2001).

Computational techniques aimed at the estimate of aggregate optical properties can be rather heavy. To overcome computational difficulties, effective medium theories (EMTs)

[1] Istituto Nazionale di Fisica della Materia, Unitá di Messina, Italy.

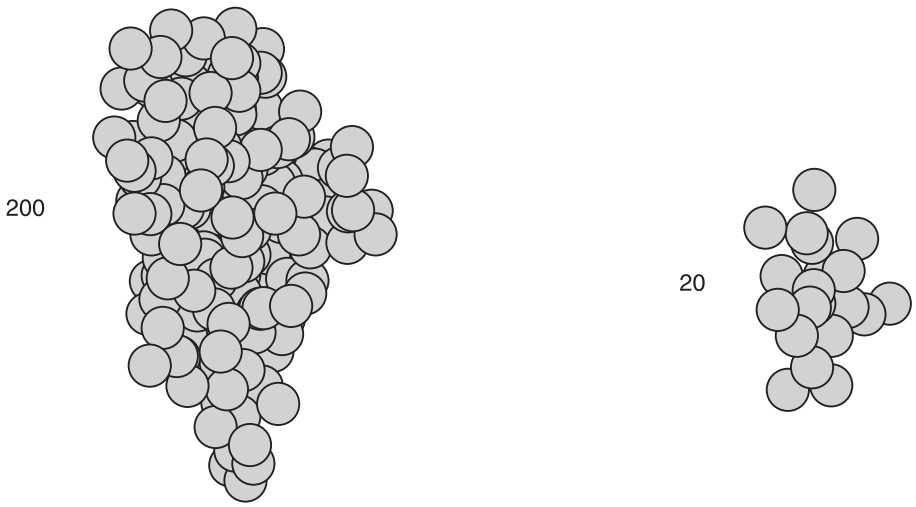

FIG. 1.—Geometry of the 200 sphere BPCA aggregate, after the accretion process is completed. The starting cluster of 20 spheres is also shown.

are often used in the literature. Any EMT unfortunately involves heavy approximations on the dielectric functions that may not be completely satisfied (Chylek et al. 2000). In fact, despite the extensive use of EMTs in the literature, basic questions regarding their applicability have remained (Wolff et al. 1998). More sophisticated approaches rely on a finite-element method, e.g., the discrete dipole approximation (DDA; Purcell & Pennypacker 1973; Draine 1988), statistical techniques, e.g., the Strong Permittivity Fluctuation Theory (SPFT; Michel et al. 1996), and exact methods (Gérardy & Ausloos 1982; Borghese et al. 2002). In this work, we investigate how modifications in the geometry of grain aggregates induce detectable changes in their optical signatures. Using the vector multipole field expansion of the electromagnetic field in the framework of the transition matrix approach (Waterman 1971), we compute the optical properties of morphologically complex particles in which the building blocks of the cluster keep their individual structure. This is a task that effective medium theories are unable to address, because material interfaces and shapes are smeared out in a homogeneous mixture. In §§ 3, 4, and 5 we present a brief outline of the method, together with a description of computational approximations and shortcuts, convergency criteria, and a comparison with other techniques. Section 6 contains a collection of results, while the conclusions we reach are presented in § 7.

2. THE AGGREGATION MODEL

We identify two main mechanisms leading to the formation of grains in dense regions: accretion of atoms and molecules in gas phase onto dust grains, forming icy mantles, and coagulation of grains upon collision. Draine (1985a) proved that the gas accretion mechanism alone fails to explain the relevant growth of dust that is inferred by the extinction curve. Coagulation then appears as a more reliable mechanism to explain the grain spectrum in such dense regions (Chokshi et al. 1993). There is no direct observational evidence of the final result of the aggregation process. Wurm & Schnaiter (2002) argue against the existence of dust aggregates composed of a great number of monomers and suggest small clusters, up to 8–16 monomers, as good candidates to explain relevant observables, such as the observed linear correlation between the total to selective extinction and the wavelength of the maximum polarization. According to the Wurm & Schnaiter (2002) calculations, large clusters fail to explain the observed polarization effects since the polarization induced by the special shape and orientation of a monomer is balanced by the polarization due to another monomer with opposite orientation. On the other side, theoretical expectations exist that coagulation is a very efficient mechanism for producing large aggregates composed of some hundreds or even thousands of subgrains in regions with gas densities larger than a million hydrogen nuclei per cubic centimeter (Ossenkopf 1993).

In our computations we adopt two different models of cluster growth: first via single-particle aggregation and then through cluster-cluster aggregation. Each step in the single-particle aggregation process is characterized by the accretion of 20 spherical monomers on the surface of the cluster resulting from the previous step, until we reach the final configuration shown in Figure 1 and made of 200 monomers (ballistic particle-cluster aggregation, BPCA). In the case of ballistic cluster-cluster aggregation (BCCA), the building blocks are groups of 20 coalesced spheres with an overall compact morphology. We assume that two such groups move along straight trajectories, undergo collisions, and stick together at their first contact point. Figure 2 shows the sequence of shots in the random coagulation process, ending up again with a final cluster of 200 spheres with an asymmetric geometry. The monomers, forming both BPCA and BCCA clusters, have identical radii of 5 nm. The resulting BPCA clusters have somewhat more compact structures with respect to BCCA clusters. In Table 1 we report some parameters characterizing the various aggregate samples (Mukai et al. 1992):

1. The radius of gyration

$$r_g = \left[\frac{1}{2N^2} \sum_{i=1}^{N} \sum_{j=1}^{N} \left(\boldsymbol{r}_i - \boldsymbol{r}_j \right)^2 \right]^{1/2}, \tag{1}$$

where N is the number of monomers in the aggregate and $\boldsymbol{r}_i$ and $\boldsymbol{r}_j$ are the position vectors of the ith and jth constituent particles, respectively.

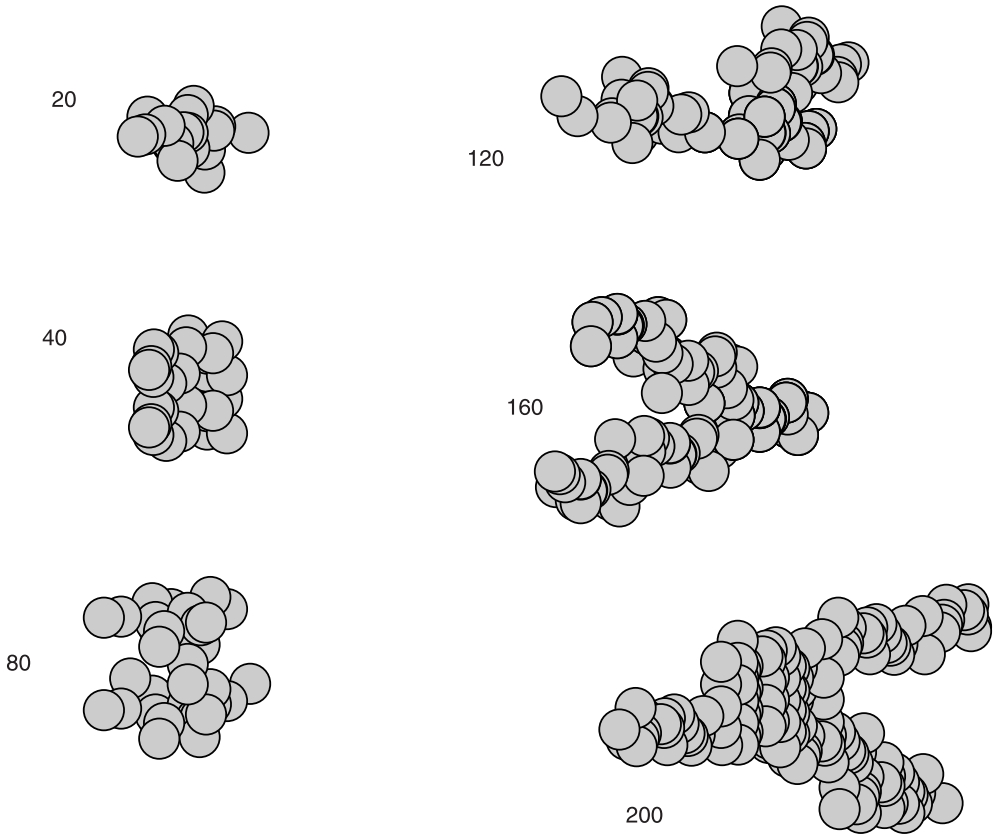

FIG. 2.—Steps during the cluster-cluster aggregation process, starting from the 20 sphere cluster and ending up with the 200 sphere BCCA aggregate.

2. The radius of the homogeneous sphere with same radius of gyration as the aggregate,

$$r_e = \sqrt{\frac{5}{3}} r_g. \tag{2}$$

3. The porosity

$$p_0 = 1 - \left(\frac{V_i}{V}\right), \tag{3}$$

where $V_i = N(4/3)\pi r_0^3$, r_0 being the radius of the constituent monomer and V being the volume of the sphere with radius r_e.

4. The fractal dimension D that is obtained as the slope of the curve of $\log N$ versus $\log (r_g/r_0)$. Since we are using a relatively small number of spheres ($N \leq 200$), we do not reach the fractal limit for either cluster model.

3. THE SCATTERING AMPLITUDE AND OPTICAL PROPERTIES

When dealing with scattering problems, the most important quantity from an observational point of view is the scattering amplitude. In fact this quantity, which gives the field scattered by a particle in the far zone, is directly related to all the quantities of interest. Let us assume that the particle is embedded in a homogeneous, nonabsorptive medium of refractive index n. The polarization both of the incident and of the scattered field is described with respect to the plane of scattering, i.e., the plane that is defined by the direction of incidence $\hat{\boldsymbol{k}}_I$ and of scattering $\hat{\boldsymbol{k}}_S$. We define two pairs of mutually orthogonal unit vectors $\hat{\boldsymbol{u}}_{I\eta}$ and $\hat{\boldsymbol{u}}_{S\eta}$, $(\eta = 1, 2)$, chosen

TABLE 1
PARAMETERS CHARACTERIZING THE CLUSTERS THAT WE USED IN OUR COMPUTATIONS

	BPCA D = 2.3			BCCA D = 1.5		
N	r_g	r_e	p_0	r_g	r_e	p_0
20	14.7	19.0	0.64	14.7	19.0	0.64
40	28.9	37.3	0.95	26.8	34.6	0.94
80	29.8	38.4	0.96	43.2	55.7	0.99
120	34.7	44.7	0.97	53.6	69.1	0.99
160	39.4	50.9	0.98	65.9	85.1	0.99
200	41.9	54.1	0.98	66.7	86.1	0.99

NOTE.—All the radii are in nm.

so that $\hat{\boldsymbol{u}}_{I2}$ and $\hat{\boldsymbol{u}}_{S2}$ are orthogonal to the plane of scattering and so oriented that

$$\hat{\boldsymbol{u}}_{I1} \times \hat{\boldsymbol{u}}_{I2} = \hat{\boldsymbol{k}}_I, \quad \hat{\boldsymbol{u}}_{S1} \times \hat{\boldsymbol{u}}_{S2} = \hat{\boldsymbol{k}}_S.$$

The incident field is assumed to be the plane-polarized wave

$$\boldsymbol{E}_{I\eta} = E_0 \hat{\boldsymbol{u}}_{I\eta} \exp(i\boldsymbol{k}_I \cdot \boldsymbol{r}),$$

where $\boldsymbol{k}_I = k\hat{\boldsymbol{k}}_I$, $k = nk_v$, with $k_v = \omega/c$ being the propagation vector. In turn, the scattered field in the far zone can be written (Jackson 1975)

$$\boldsymbol{E}_{S\eta} = E_0 \frac{e^{ikr}}{r} \boldsymbol{f}_\eta(\hat{\boldsymbol{k}}_S, \hat{\boldsymbol{k}}_I), \tag{4}$$

where $\boldsymbol{f}$ is the scattering amplitude and the subscript η recalls the polarization of the incident field. Once the scattering amplitude is known, the scattering cross section turns out to be

$$C_{S\eta} = \int_{\Omega_S} \left|\boldsymbol{f}_\eta(\hat{\boldsymbol{k}}_S, \hat{\boldsymbol{k}}_I)\right|^2 d\Omega_S,$$

where the integral is over the direction of the scattered wavevector. The optical theorem gives the extinction cross section

$$C_{T\eta} = \frac{4\pi}{k} \operatorname{Im}\left[\boldsymbol{f}_\eta(\hat{\boldsymbol{k}}_S = \hat{\boldsymbol{k}}_I, \hat{\boldsymbol{k}}_I) \cdot \hat{\boldsymbol{u}}_{I\eta}\right].$$

In turn, the albedo is given by

$$\varpi_\eta = \frac{C_{S\eta}}{C_{T\eta}},$$

and the asymmetry parameter can be easily calculated as

$$g_\eta = \frac{1}{k^2 C_{S\eta}} \int_{\Omega_S} \left|\boldsymbol{f}_\eta(\hat{\boldsymbol{k}}_S, \hat{\boldsymbol{k}}_I)\right|^2 \hat{\boldsymbol{k}}_S \cdot \hat{\boldsymbol{k}}_I \, d\Omega_S,$$

where

$$\hat{\boldsymbol{k}}_S \cdot \hat{\boldsymbol{k}}_I = \cos\Phi,$$

Φ being the angle of scattering. Finally, all these ingredients give the radiation pressure cross section

$$C_{\mathrm{pr}\,\eta} = C_{T\eta} - g_\eta C_{S\eta}.$$

All the quantities defined above refer to particles of general shape and thus depend on the polarization of the incident field, as explicitly indicated by the subscript η.

To compute all these quantities we use the transition matrix method. We expand the incident field $\boldsymbol{E}_{I\eta}$ in a series of vector multipole fields as (Borghese et al. 2002)

$$\boldsymbol{E}_{I\eta}(\boldsymbol{r}) = E_0 \sum_{plm} \boldsymbol{J}_{lm}^{(p)}(\boldsymbol{r}, k) W_{I\eta lm}^{(p)}, \tag{5}$$

where $\boldsymbol{J}_{lm}^{(p)}$ denotes the vector multipole fields

$$\boldsymbol{J}_{lm}^{(1)}(\boldsymbol{r}, k) = j_l(kr)\boldsymbol{X}_{lm}(\hat{\boldsymbol{r}}),$$

$$\boldsymbol{J}_{lm}^{(2)}(\boldsymbol{r}, k) = \frac{1}{k} \nabla \times \boldsymbol{J}_{lm}^{(1)}(\boldsymbol{r}, k)$$

that are regular at the origin. In the preceding equations the vector functions $\boldsymbol{X}_{lm}$ are vector spherical harmonics (Jackson 1975), j_l are spherical Bessel functions, and the superscript p is a parity index that distinguishes the magnetic multipoles ($p = 1$) from the electric ones ($p = 2$). In turn $W_{I\eta lm}^{(p)} = W_{lm}^{(p)}(\hat{\boldsymbol{u}}_{I\eta}, \hat{\boldsymbol{k}}_I)$, with

$$W_{lm}^{(p)}(\hat{\boldsymbol{e}}, \hat{\boldsymbol{k}}) = 4\pi i^{p+l-1} \hat{\boldsymbol{e}} \cdot \boldsymbol{Z}_{lm}^{(p)*}(\hat{\boldsymbol{k}}),$$

where $\boldsymbol{Z}_{lm}^{(p)}(\hat{\boldsymbol{k}})$ are the transverse harmonics (Fucile et al. 1997)

$$\boldsymbol{Z}_{lm}^{(1)}(\hat{\boldsymbol{k}}) = \boldsymbol{X}_{lm}(\hat{\boldsymbol{k}}), \quad \boldsymbol{Z}_{lm}^{(2)}(\hat{\boldsymbol{k}}) = \boldsymbol{X}_{lm}(\hat{\boldsymbol{k}}) \times \hat{\boldsymbol{k}}.$$

The scattered field is expanded as

$$\boldsymbol{E}_{S\eta} = E_0 \sum_{plm} \boldsymbol{H}_{lm}^{(p)}(\boldsymbol{r}, k) A_{\eta lm}^{(p)}, \tag{6}$$

where $\boldsymbol{H}_{lm}^{(p)}$ denote multipole fields that are identical to the $\boldsymbol{J}$ multipole fields except for the substitution of the Hankel functions of the first kind h_l in place of the Bessel functions j_l and thus satisfy the radiation condition at infinity.

At this stage we introduce the transition matrix of the scattering particle as the operator that, acting on the known multipole amplitudes of the incident field $W_{I\eta lm}^{(p)}$, gives the amplitudes of the scattered field. In fact, the linearity of the Maxwell equations and of the boundary conditions across the surface of the particle grants the definition of the elements of the transition matrix according to the equation (Waterman 1971)

$$A_{\eta lm}^{(p)} = \mathcal{S}_{lml'm'}^{(pp')} W_{I\eta l'm'}^{(p')}. \tag{7}$$

The elements of the transition matrix $\mathcal{S}_{lml'm'}^{(pp')}$ encompass all the information on the morphology and orientation of the particle with respect to the incident field, and their relation to the scattering amplitude can be established by noting that, for large r, i.e., in the far field zone, the asymptotic form of the $\boldsymbol{H}$ multipole fields is (Abramowitz & Stegun 1965)

$$\boldsymbol{H}_{lm}^{(p)}(\boldsymbol{r}, k) \to (-i)^{l+p} \frac{e^{ikr}}{r} \boldsymbol{Z}_{lm}^{(p)}(\hat{\boldsymbol{k}}_S). \tag{8}$$

Then, by substituting equation (8) into equation (6) and using equation (4) and the definition equation (7), we get (Borghese et al. 2002)

$$\boldsymbol{f}_\eta = \frac{1}{k} \sum_{plm} \sum_{p'l'm'} (-i)^{l+p} \boldsymbol{Z}_{lm}^{(p)}(\hat{\boldsymbol{k}}_S) \mathcal{S}_{lml'm'}^{(pp')} W_{l'm'}^{(p')}(\hat{\boldsymbol{u}}_{I\eta}, \hat{\boldsymbol{k}}_I). \tag{9}$$

The transition matrix approach presents invaluable advantages when dealing with the properties of dispersions of particles whose orientational distribution is known because the transition matrix has well-defined transformation properties under rotation that permit a straightforward (analytical) evaluation of orientational averages (Borghese et al. 1984, 2001, 2002). In fact, since we are interested in the optical properties of dispersions as a whole, we exploit these properties assuming a random orientational distribution. The analytical evaluation of the averages produces a much improved accuracy of the solution and results in a remarkable reduction of CPU time. In the simple case of a random orientational distribution, Mishchenko & Mackowski (1996) estimate that the CPU time needed for the analytical evaluation of the orientational averages is a factor of thousands shorter than that required by a numerical evaluation.

4. THE CLUSTER MODEL

The transition matrix approach is suitable for calculating the scattering amplitude of composite nonspherical particles, and in particular of particles modeled as aggregates of spheres. We thus consider an aggregate of spheres, numbered by the index α, of radius ρ_α and refractive index n_α whose centers lie at $\boldsymbol{R}_\alpha$, embedded in a nonabsorptive medium of refractive index n. Neither the radii nor the refractive indexes of the component spheres need to be equal to each other. The polarized plane wave field $\boldsymbol{E}_{I\eta}$ impinging on the aggregate is expanded as in the preceding section. In turn, the field scattered by the entire aggregate is written as the superposition of the fields scattered by the single spheres:

$$\boldsymbol{E}_{S\eta} = E_0 \sum_\alpha \sum_{plm} \boldsymbol{H}_{lm}^{(p)}(\boldsymbol{r}_\alpha, k)\mathcal{A}_{\eta\alpha lm}^{(p)}, \tag{10}$$

where $\boldsymbol{r}_\alpha = \boldsymbol{r} - \boldsymbol{R}_\alpha$, whereas the field within the αth sphere is expanded as

$$\boldsymbol{E}_{T\eta\alpha} = E_0 \sum_{plm} \boldsymbol{J}_{lm}^{(p)}(\boldsymbol{r}_\alpha, k_\alpha)\mathcal{C}_{\eta\alpha lm}^{(p)}. \tag{11}$$

The amplitudes $\mathcal{A}_{\eta\alpha lm}^{(p)}$ and $\mathcal{C}_{\eta\alpha lm}^{(p)}$ in equations (10) and (11) are determined by the boundary conditions across the surface of each sphere in the cluster, and knowing them totally solves the problem of the dependent scattering from the aggregate. In fact, using the procedure that is described by Borghese et al. (1984), the amplitudes $\mathcal{A}_{\eta\alpha lm}^{(p)}$ turn out to be the solution to the system of linear nonhomogeneous equations

$$\sum_{\alpha'} \sum_{p'l'm'} \mathcal{M}_{\alpha lm\alpha' l' m'}^{(pp')}\mathcal{A}_{\eta\alpha' l' m'}^{(p')} = -\mathcal{W}_{\eta\alpha lm}^{(p)}, \tag{12}$$

where we define the *shifted* amplitudes of the incident field

$$\mathcal{W}_{\eta\alpha lm}^{(p)} = \sum_{p'l'm'} \mathcal{J}_{\alpha lm0l'm'}^{(pp')} W_{I\eta l'm'}^{(p')}, \tag{13}$$

$$\mathcal{M}_{\alpha lm\alpha' l' m'}^{(pp')} = \left(R_{\alpha l}^{(p)}\right)^{-1} \delta_{\alpha\alpha'}\delta_{pp'}\delta_{ll'}\delta_{mm'} + \mathcal{H}_{\alpha lm\alpha' l' m'}^{(pp')}. \tag{14}$$

In the preceding equations the quantities $\mathcal{J}_{\alpha lm0l'm'}^{(pp')}$ are the elements of the matrix that, according to the addition theorem for multipole fields (Borghese et al. 1980, 2002), translates these fields from the origin of the coordinates O at $\boldsymbol{R}_0 = 0$ to $\boldsymbol{R}_\alpha$, i.e., to the center of the αth sphere; the quantities $R_{\alpha l}^{(1)}$ and $R_{\alpha l}^{(2)}$, except for a sign, are the elements of the transition matrix for the αth sphere and coincide with the customary Mie coefficients b_l and a_l, respectively; also, the quantities $\mathcal{H}_{\alpha lm\alpha' l' m'}^{(pp')}$, whose explicit expression is given by Borghese et al. (1994), come from the addition theorem for vector multipole fields (Borghese et al. 1980, 2002) and take account of the multiple scattering processes that occur among the spheres in the aggregate.

In order to calculate the transition matrix of the entire aggregate, let $\mathbf{M}$ be the matrix whose elements are given by equation (14). Then the formal solution to system (12) is

$$\mathcal{A}_{\eta\alpha lm}^{(p)} = -\sum_{p'l'm'} \left(\mathbf{M}^{-1}\right)_{\alpha lm\alpha' l' m'}^{(pp')} \mathcal{W}_{\eta\alpha' l' m'}^{(p')}. \tag{15}$$

Furthermore, the above-mentioned addition theorem allows us to write the scattered field, equation (10), in terms of multipole fields with origin at O as

$$\begin{aligned}\boldsymbol{E}_{S\eta} &= E_0 \sum_{plm} \sum_{\alpha'} \sum_{p'l'm'} \boldsymbol{H}_{lm}^{(p)}(\boldsymbol{r}, k)\mathcal{J}_{0lm\alpha' l' m'}^{(pp')}\mathcal{A}_{\eta\alpha' l' m'}^{(p')} \\ &= \sum_{plm} \boldsymbol{H}_{lm}^{(p)}(\boldsymbol{r}, k)A_{\eta lm}^{(p)},\end{aligned} \tag{16}$$

where we define

$$A_{\eta lm}^{(p)} = \sum_{\alpha'} \sum_{p'l'm'} \mathcal{J}_{0lm\alpha' l' m'}^{(pp')}\mathcal{A}_{\eta\alpha' l' m'}^{(p')}, \tag{17}$$

and the quantities $\mathcal{J}_{0lm\alpha' l' m'}^{(pp')}$ are the elements of the matrix that translates the origin of the $\boldsymbol{H}$ multipole fields from $\boldsymbol{R}_{\alpha'}$ to the origin of the coordinates at O. We stress that equation (16) is valid outside the smallest sphere that contains the entire aggregate and is thus appropriate to get the scattered field in the far zone. In fact, according to equations (7), (13), (15), and (17), the transition matrix elements of the entire aggregate are

$$\mathcal{S}_{lml'm'}^{(pp')} = \sum_{\alpha\alpha'} \sum_{qLM} \sum_{q'L'M'} \mathcal{J}_{0lm\alpha LM}^{(pq)} \left(\mathbf{M}^{-1}\right)_{\alpha LM\alpha' L' M'}^{(qq')} \mathcal{J}_{\alpha' L' M' 0l'm'}^{(q'p')}. \tag{18}$$

Equation (18) can then be inserted into equation (9) to yield the scattering amplitude of the entire aggregate.

5. CONVERGENCE

The calculation of the transition matrix of a cluster requires inverting the matrix $\mathbf{M}$ whose order is, in principle, infinite. Of course system (12) is truncated to some finite order by including in equation (18) terms up to order L_I, the maximum value both for L and L' in equation (18). The maximum value is chosen to ensure the required accuracy of the transition matrix elements. For a cluster of N spheres this implies the solution of a system of order $D_I = 2NL_I(L_I + 2)$, which may become too large. Actually, the inversion of the matrix $\mathbf{M}$ is responsible for most of the time required for the calculation; this time scales, in fact, as D_I^3. Thus, on account of the definition of D_I, the computation time scales as L_I^6 whereas the storage requirements scale as L_I^4, so that it pays, in terms of both CPU time and storage requirements, to keep L_I as low as practicable. On the other hand, l_E, the maximum value of l and l' in equations (7), (9), and (18), can be chosen to be greater than L_I. In fact, as the main body of the calculation lies on the inversion of matrix $\mathbf{M}$, little is added to the burden of the calculation by choosing $l_E > L_I$. On the other hand, a large value of l_E improves the description of the scattered field in the far zone provided that L_I too has been chosen large enough to ensure fair convergence of the elements of the transition matrix.

The choice of the appropriate value of L_I has been the concern of several researchers. For instance Quinten et al. (2002) used the criterion suggested by Wiscombe (1979). Our choice of L_I and l_E has been guided by the following considerations. For an isolated dielectric sphere with radius b_s we have to choose $L_I > kb_s + m_s$ (Stratton 1941), where m_s is an integer that depends on the refractive index. Now, by looking to equations (12) and (14), we see that what distinguishes a set of independent spheres from a true aggregate of spheres is the presence of the elements $\mathcal{H}_{\alpha lm\alpha' l' m'}^{(pp')}$ that describe the multiple scattering processes occurring among the spheres. Of course,

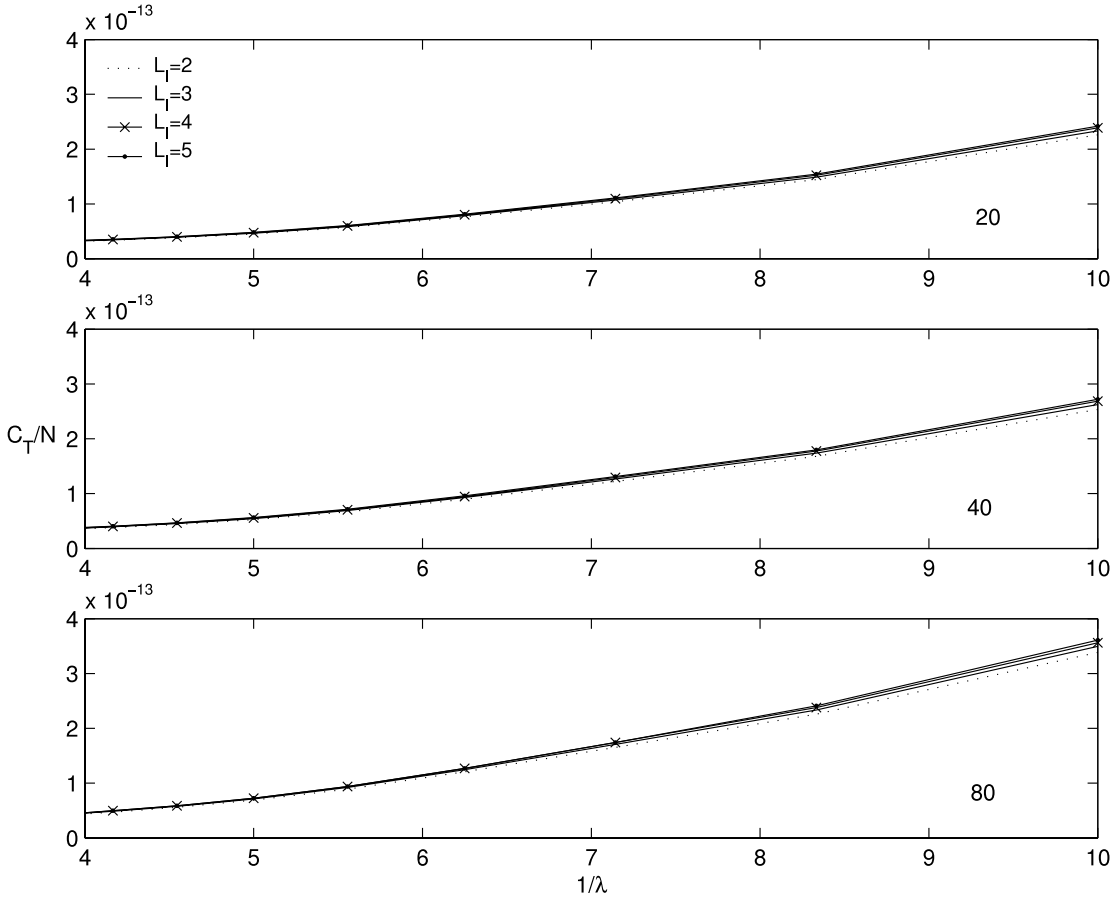

FIG. 3.—Convergence test: extinction cross sections (in cm^2) normalized to the number of spheres for BCCA aggregates of amorphous carbon. Label numbers refer to the number of spheres composing the aggregates in each panel, and $1/\lambda$ is in μm^{-1}.

these processes are bound to become less and less effective the more the spheres are separated. By looking to the explicit expression of the $\mathcal{H}$ elements (Borghese et al. 2002), one sees that their magnitudes actually become smaller and smaller for well-separated spheres. As a result, we can assume that, choosing L_I a little larger than necessary to ensure the convergence of the component spheres as if they were isolated, we should also get fairly convergent values for the transition matrix elements once we choose l_E so as to get a fair description of the field scattered by the entire cluster. Thus we make the *Ansatz* that we can choose $l_I > k_v b_c + m_c$, where b_c is the radius of the smallest sphere including the entire aggregate. Even in this case m_c is an integer that depends on the refractive index. Using this criterion Saija et al. (2003) were able to get fairly convergent results for clusters composed of 13 spheres of size parameter exceeding 13. The convergence for the aggregates that we deal with in the present paper will be discussed in the next section.

6. RESULTS: EFFECTS OF CLUSTER GROWTH

In this section we discuss the results obtained for the complete sequence of clusters during the coagulation process, for both BPCA and BCCA processes, using as grain constituents either astronomical silicates (Draine 1985b) or amorphous carbon (Rouleau & Martin 1991), or both materials.[2]

[2] We are fully aware of the existence of more recent sets of optical constants for both silicate and carbonaceous materials (e.g., Suh 1999, 2000). However, for the sake of comparison with our previous results, we continue adopting the quoted data sources.

As regards the analytic averaging procedure that we have adopted here, we add a few clarifying considerations (Borghese et al. 2002):

1. The inversion of the large matrix **M** (eq. [14]) needs to be performed only once.
2. The accuracy of the averaged results is the same as the accuracy of the results for any chosen orientation of the scatterer.

Accordingly, we follow Saija et al. (2001) and perform analytically all the orientational averages that are presented in the following figures (Borghese et al. 2002); in all cases, a random distribution of the orientations is assumed.

In § 5 we did not discuss the influence on the rate of convergence of a nonnegligible imaginary part of the refractive index of the aggregating monomers, as is indeed the case for amorphous carbon. In Figure 3 we show some results coming from our study of convergence for BCCA aggregates of amorphous carbon monomers as a function of L_I. A careful analysis shows that an increase in L_I only slightly affects the computed extinction cross sections of the aggregates. Very small variations (up to a few percent) appear only in the ultraviolet region. This makes us confident that $L_I = 2$ is also adequate for getting fairly convergent results when dealing with the largest BPCA and BCCA aggregates modeled in this paper. Running analogous tests for aggregates of silicates and aggregates with mixed chemical composition, we obtain very similar results. This suggests that the refractive index does not influence the convergence rate throughout the wavelength of

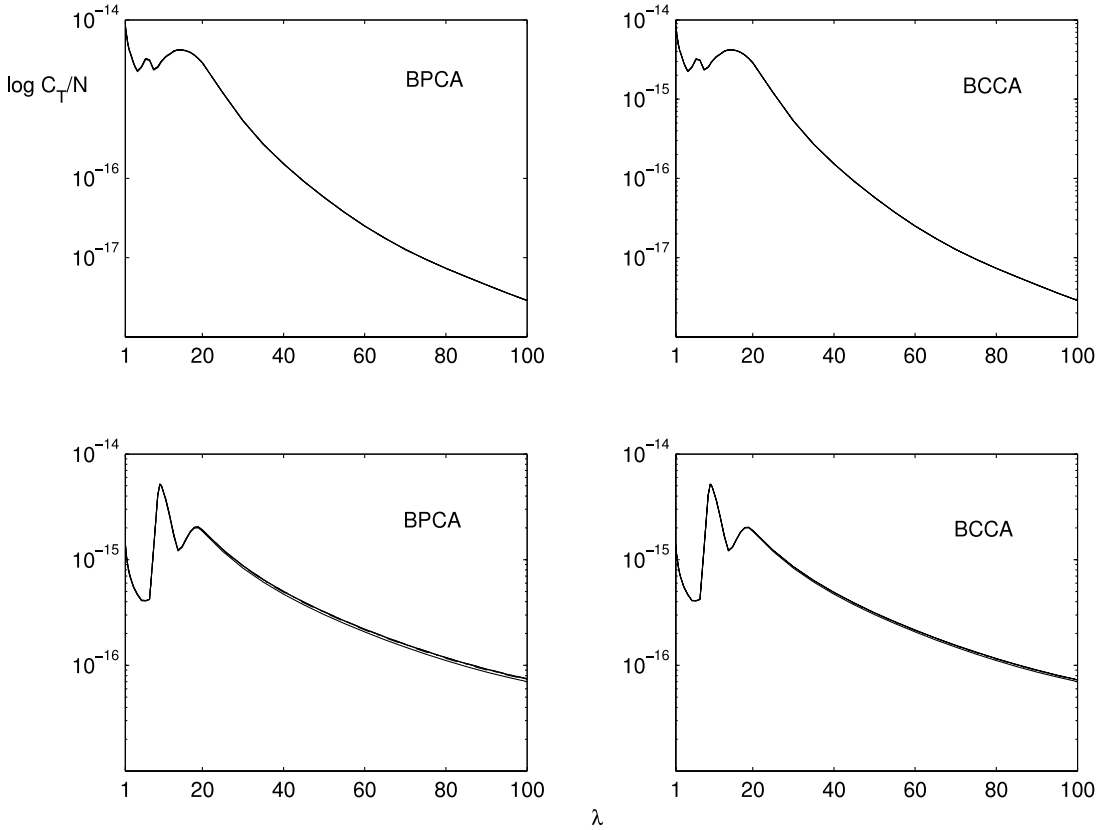

FIG. 4.—Extinction cross sections normalized to the number of spheres for BPCA and BCCA aggregates of amorphous carbon (*top*) and silicates (*bottom*) grains in the IR region of the spectrum. The curves relative to the 20-40-80-120-160-200 sphere aggregates overlap almost perfectly. The wavelength λ is in μm.

interest. With the size parameter in vacuo of the constituent monomers being $k_v b_s \leq 0.3$, in our computations we used with reasonable confidence $L_I = 2$ and $l_E = 7{-}10$. Consider that $L_I = 2$ is the value ensuring full convergence for the extinction cross sections of the spherical monomers (Saija et al. 2003).

A convenient way to highlight the role of morphology is to normalize the cross sections to the number of spheres composing the aggregates. This representation is also related to the extinction power per unit mass. We first examine the case of homogeneous chemical composition. We follow the cluster growth process starting from the 20 sphere aggregate up to the 200 sphere configuration. No valuable difference appears in the trend of the curves relative to the optical properties in the infrared region of the spectrum that we analyzed up to 100 μm, averaged for random orientations of the particles (Fig. 4). In this region the extinction cross sections scale with the mass of grains. The behavior is quite different in the ultraviolet region where multiple scattering processes among the constituent monomers shape the cross sections, depending on the details of the cluster morphology, i.e., the number of monomers and how they are arranged. In Figures 5–8 we show the extinction cross section, the radiation pressure cross section, the albedo, and the asymmetry parameter for the two adopted models and the two reference materials. Carbon grains (Figs. 5 and 6) show, in both morphological configurations, that larger clusters are more efficient in light extinction than smaller ones. Such behavior is totally absent in silicate clusters (Figs. 7 and 8), which are only slightly dependent on changes in the morphology. These considerations can be extended to the radiation pressure cross sections. As expected, albedo and the asymmetry parameter increase with increasing aggregate size, i.e., increasing numbers of constituents.

Finally, we consider BPCA aggregates presenting mixed chemical composition. During the aggregation process, a cluster grows by deposition of monomers of different materials falling in at random trajectories. The resulting aggregate contains equal volumes of silicate and carbonaceous components. In Figure 9 we compare the extinction cross section, the radiation pressure cross section, the albedo, and the asymmetry parameter of random dispersions of grain aggregates composed by 80 monomers of mixed chemical composition with the corresponding quantities computed for homogeneous silicate and carbonaceous grain aggregates. As expected, the optical behavior of the inhomogeneous aggregate is intermediate between the two homogeneous cases.

Is clustering synonymous with enhanced extinction power? The answer to this question is related to the size parameters of both aggregate and constituent subunits. As a consequence there are no general recipes for composite grains. For our set of calculations, a comparison among the extinction cross sections relative to BPCA and BCCA aggregates and the homogeneous single spheres of equivalent mass (amorphous carbon particles [Fig. 10] and silicate particles [Fig. 11]) gives straightforward insight into the effect of morphology on the optical properties of such grain aggregates. The equivalent-mass sphere is in general comparable, if not more efficient, in extinguishing radiation than aggregates, at least in the visible-ultraviolet spectral range. This is a direct consequence of the smaller size of the equivalent sphere, which approaches more closely the dimension of the wavelength of the incident radiation.

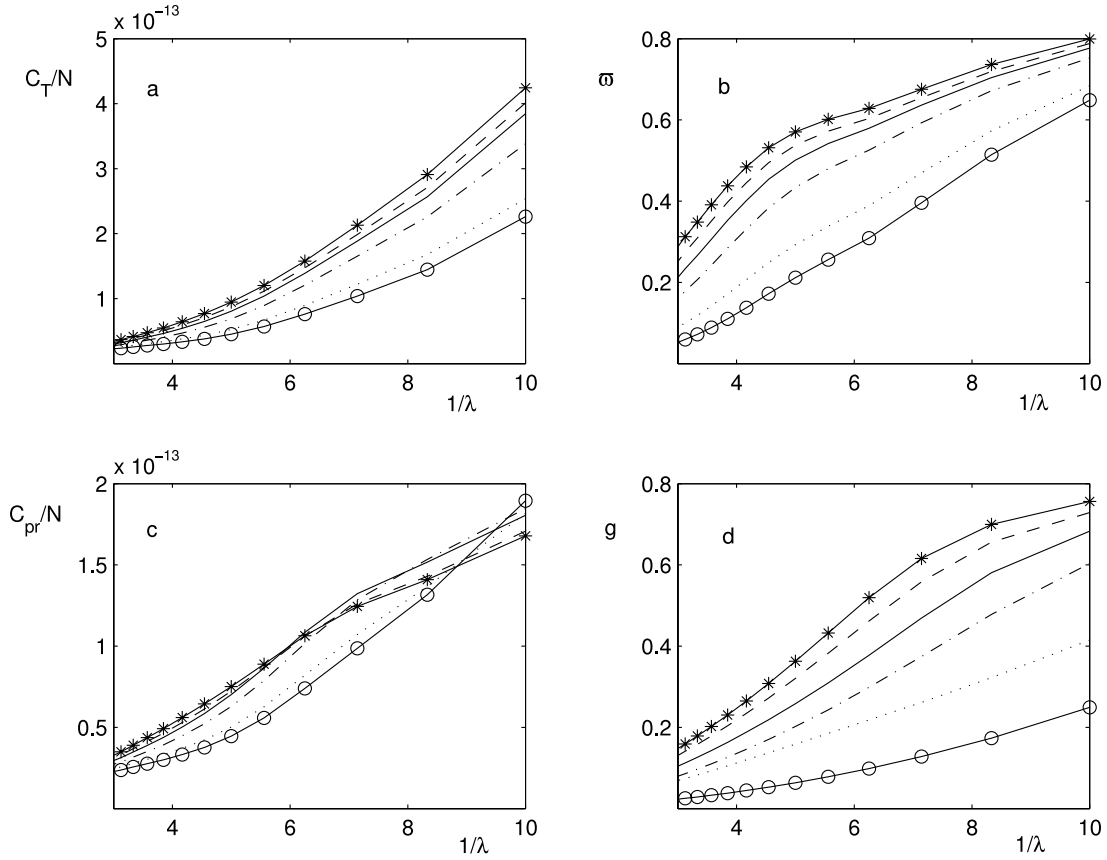

FIG. 5.—(*a*) Extinction and (*c*) radiation pressure cross sections (in cm^2) normalized to the number of spheres, (*b*) albedo, and (*d*) asymmetry parameter for BPCA aggregates of amorphous carbon grains. The quantity $1/\lambda$ is in μm^{-1}. *Solid line with circles*: 20 spheres. *Dotted line*: 40 spheres. *Dash-dotted line*: 80 spheres. *Solid line*: 120 spheres. *Dashed line*: 160 spheres. *Solid line with asterisks*: 200 spheres.

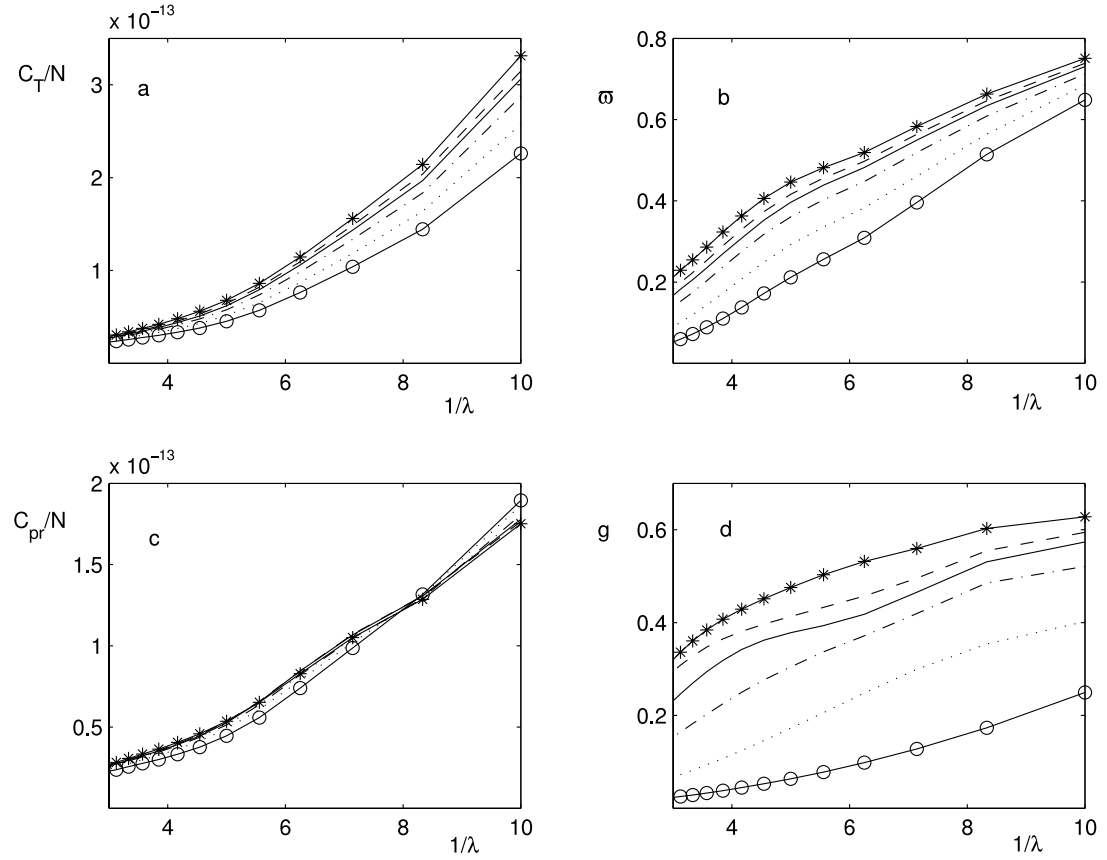

FIG. 6.—Same as Fig. 5, but for BCCA aggregates of amorphous carbon grains.

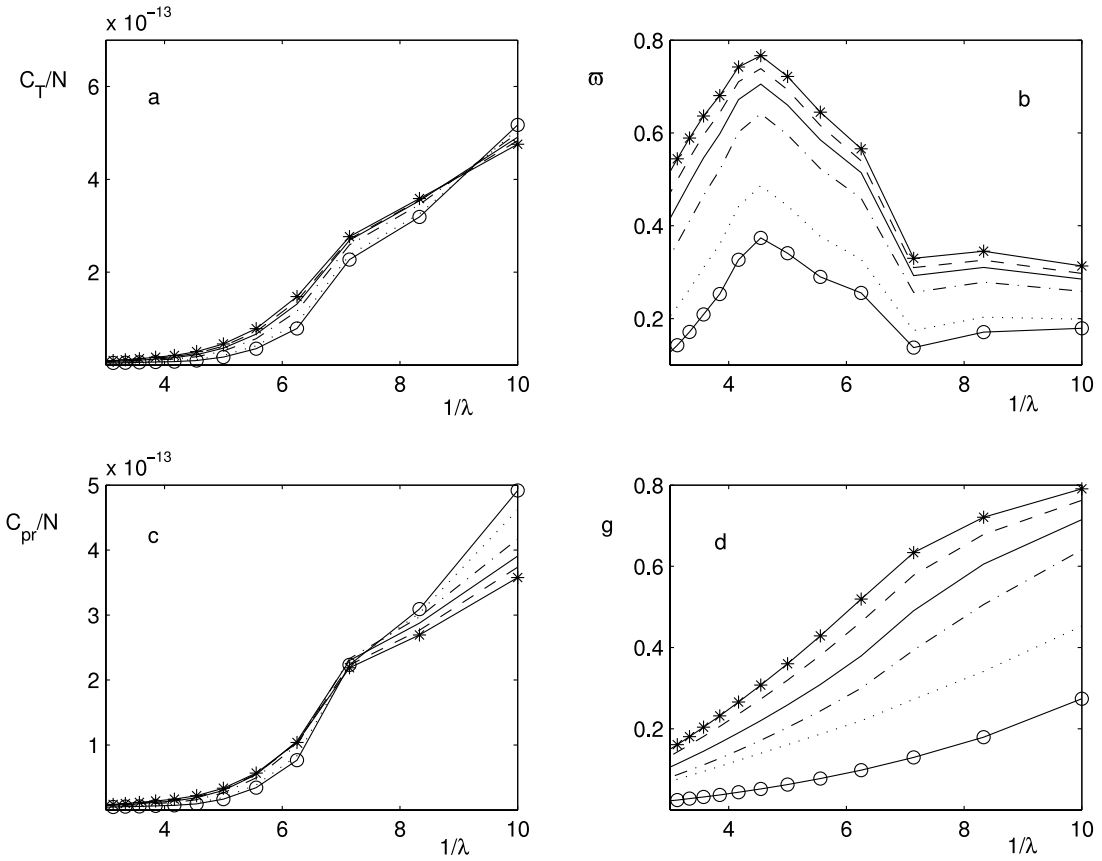

FIG. 7.—Same as Fig. 5, but for BPCA aggregates of silicate grains.

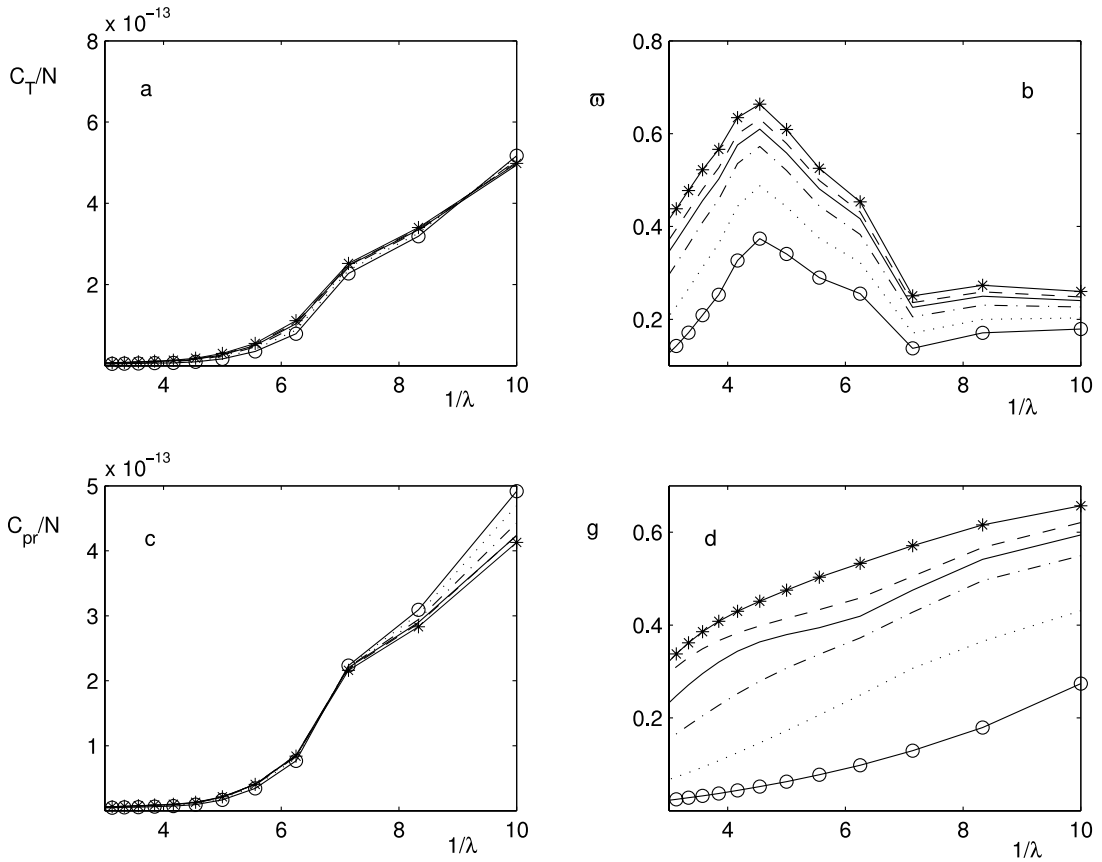

FIG. 8.—Same as Fig. 5, but for BCCA aggregates of silicate grains.

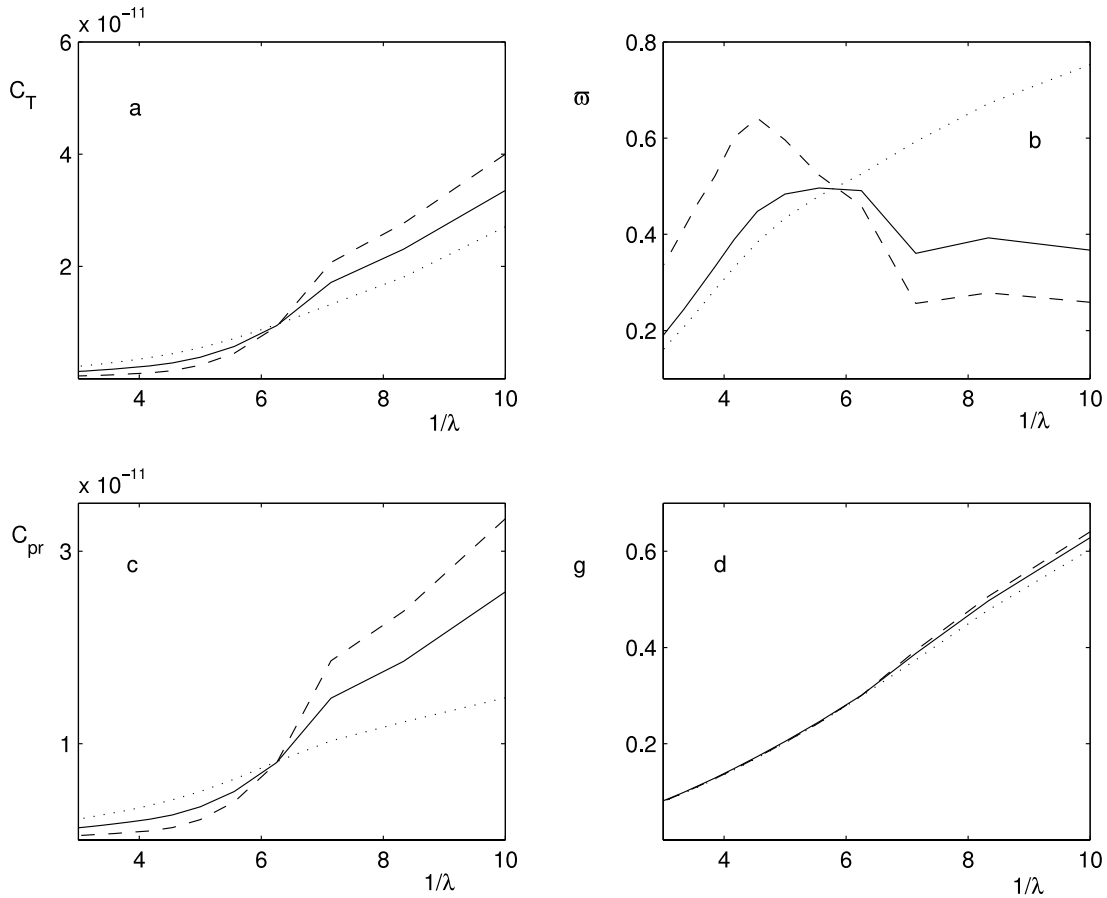

FIG. 9.—(*a*) Extinction and (*c*) radiation pressure cross sections (in cm^2), (*b*) albedo, and (*d*) asymmetry parameter for BPCA 80 monomer aggregate of mixed chemical composition (*solid line*) compared with 80 monomer amorphous carbon aggregate (*dotted line*) and 80 monomer silicate aggregate (*dashed line*). The quantity $1/\lambda$ is in μm^{-1}.

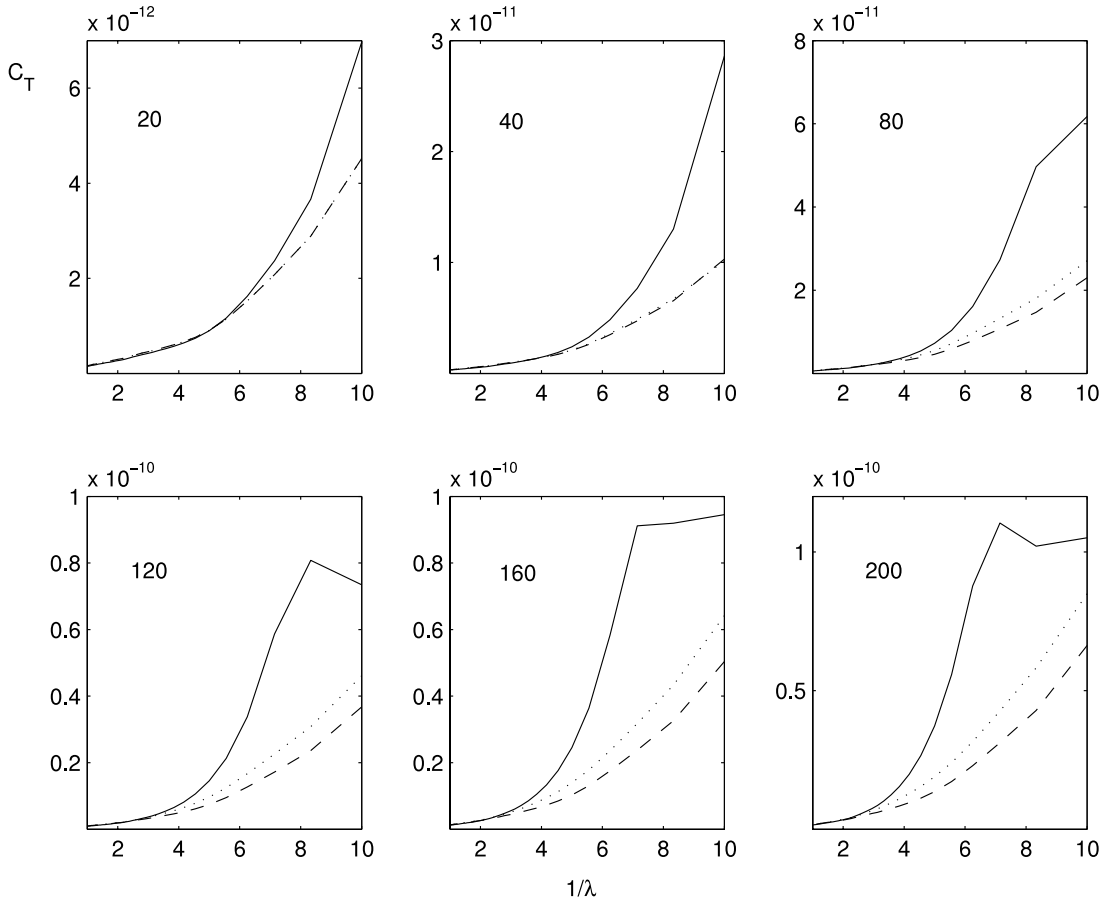

FIG. 10.—Extinction cross sections (in cm^2) for BPCA aggregate (*dotted line*), BCCA aggregate (*dashed line*), and corresponding equivalent-mass sphere (*solid line*). Grains are made of amorphous carbon. Label numbers refer to the number of spheres composing the aggregates, and $1/\lambda$ is in μm^{-1}.

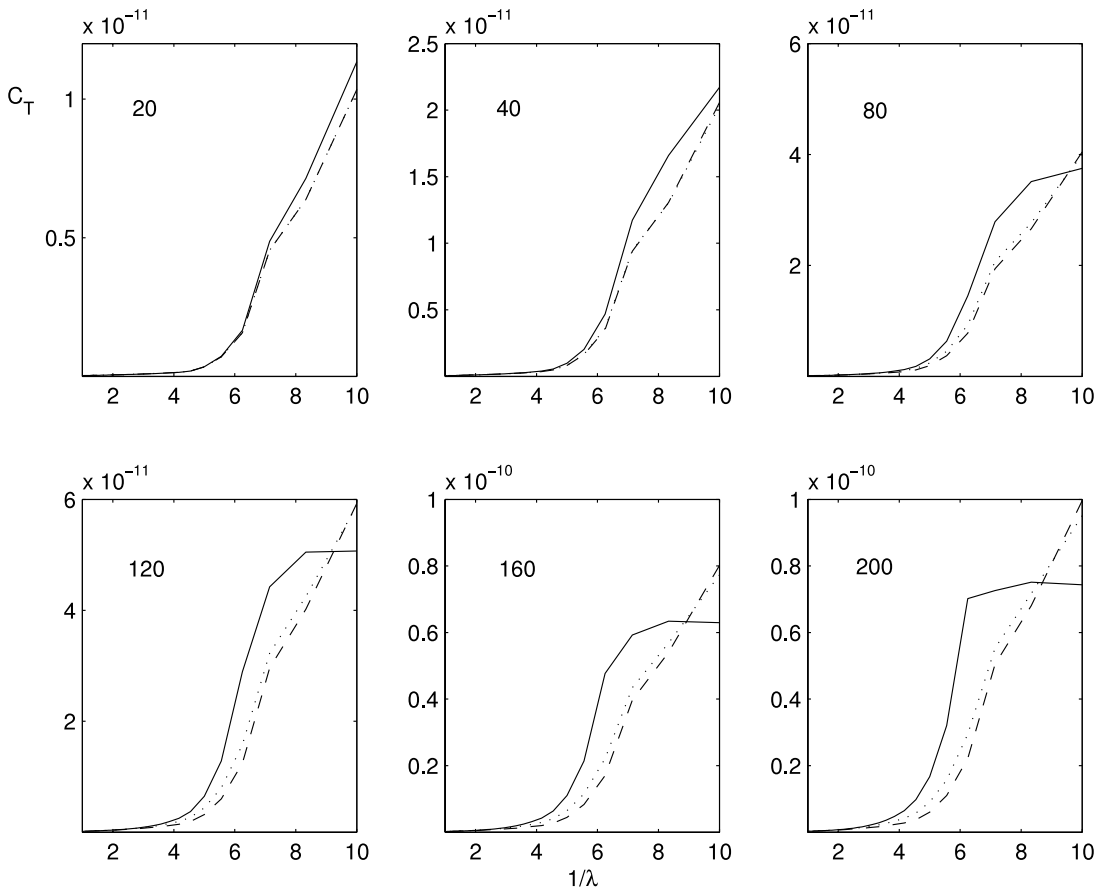

FIG. 11.—Same as Fig. 10, but for silicate dust grains.

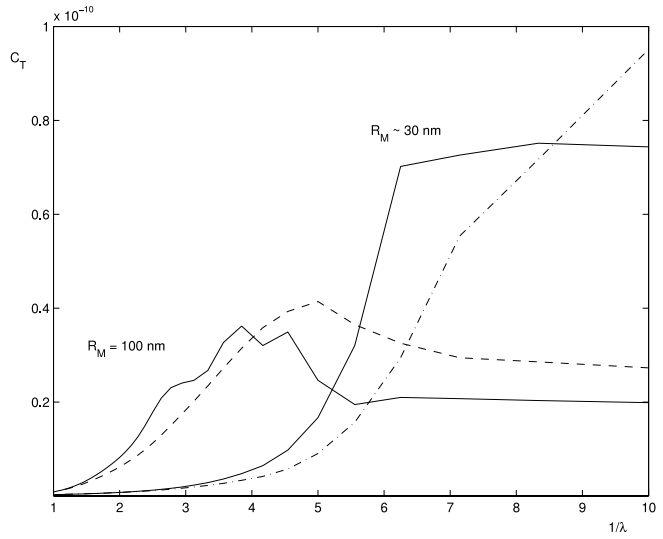

FIG. 12.—Normalized extinction cross sections (in cm^2) for BPCA 12 monomer aggregate (*dashed line*) compared with the 200 monomer aggregate (*dash-dotted line*). Labeled solid lines indicate homogeneous silicate spheres of radii $R_M \sim 30$ and 100 nm, and $1/\lambda$ is in μm^{-1}.

Our adopted model aggregates are quite different from the models derived by Wurm & Schnaiter (2002) from dichroic extinction observations, i.e., aggregates composed of a small number of large-sized monomers. Such large composite particles have large-sized parameters and turn out to be more effective in extinguishing radiation at larger wavelengths than the aggregates considered so far. We thus consider a BPCA silicate cluster assembled with 12 monomers of radii 50 nm, and we compare in Figure 12 the extinction cross sections with those relative to the equivalent-mass sphere of radius $R_M = 100$ nm. In the same figure we also show, for the sake of comparison, the extinction cross sections relative to the BPCA aggregate of 200 silicate spheres with radii of 5 nm and the corresponding equivalent-mass sphere ($R_M \sim 30$ nm). The cross sections of the larger mass cluster have been scaled of a factor of 40, corresponding to the mass ratio of the two aggregates. As expected, the 12 monomer cluster presents larger extinction cross sections in the visible/infrared portion of the spectrum, while the 200 monomer cluster dominates in the ultraviolet. However, in the relevant spectral ranges, i.e., visible/infrared for the 12 monomer cluster and ultraviolet for the 200 monomer cluster, the corresponding equal-mass spheres exhibit comparable if not larger extinction cross sections. These results suggest that the presence of aggregation cannot give a larger extinction cross section per unit mass with respect to the homogeneous sphere, as inferred in previous calculations based on EMT (Mathis 1996).

7. CONCLUSIONS

In this work we have explored the possibility that interstellar grains are composites of a large number of very small subunits (Mathis & Whiffen 1989; Mathis 1996) and we have computed the relevant optical quantities as a function of the number of constituents. Since a detailed exact treatment of extinction cross sections is mandatory for a correct understanding of the nature of interstellar dust, we exploit the T-matrix technique based on the multipole expansions of the electromagnetic field, which has proven to be general, flexible, and powerful in treating scattering of light by composite, arbitrarily shaped particles (Borghese et al. 2002).

A number of papers are present in the literature computing extinction cross sections of *true* composite interstellar grains, i.e., grain models in which the basic building blocks retain their individuality. Several of them exploit DDA-derived techniques, e.g., Vaidya et al. (2001), while others develop models for light scattering and absorption by aggregates of spheres, e.g., Saija et al. (2001) and Quinten et al. (2002). The computed cross sections depend on the morphology of the aggregate and the orientation of the composite particle with respect to the incident light. For dispersions of particles with random orientations, a large number of calculations are necessary to obtain orientational averages (Quinten et al. 2002), unless analytical procedures are available (Saija et al. 2001).

In this work, by means of the transformation properties under rotation of the transition matrix, together with an astute choice of the truncation indexes L_I and l_E, we have been able to perform a morphological analysis of the optical properties of aggregates composed by relatively large numbers of small-sized components (up to $N = 200$) without loss of accuracy and in a reasonable amount of CPU time. Since aggregates composed by a small number of large-sized monomers appear consistent with interstellar dust polarization observables (Wurm & Schnaiter 2002), we compute their relevant optical cross sections as well and then present a number of cross-comparisons between composite particles and their corresponding equal-mass spheres.

The general results from this work are as follows:

1. The extinction, scattering, and radiation pressure cross sections appear to be only slightly dependent on the shape of carbon aggregates; i.e., BPCA aggregates differ little from BCCA aggregates composed of the same numbers of monomers. For aggregates composed of silicate spheres as basic constituents, no significant differences are present.
2. An increase in the number of constituent monomers in carbonaceous aggregates produces larger extinction cross sections per unit mass (or unit volume); again, silicate materials show no significant variations.
3. For wavelengths larger than 0.25 μm ($1/\lambda < 4\ \mu m^{-1}$), no valuable differences appear in the trend of the extinction cross sections per unit mass of amorphous carbon aggregates; we do not find trends similar to the ones found by Quinten et al. (2002) in the infrared in the case of cross sections per unit volume of compact carbonaceous aggregates. Such different far-IR trends may be due to the use of different refractive indices for carbon.
4. The optical properties of mixed chemical composition (50% amorphous carbon and 50% silicate materials) aggregates are intermediate between those of homogeneous aggregates composed of the same number of basic constituents.
5. Equivalent-mass spheres are in general comparable or even more efficient in the extinction of radiation than corresponding equal-mass aggregates.

These conclusions can be affected by the limited (even if large) number of simulations. As a general result, the extinction cross sections show that the effect of the subdivision and clustering is quite different in different spectral regions. The origin of this behavior can be traced back to the multiple scattering processes that occur among the components of an aggregate. These processes appear to give a more effective contribution when the wavelength is of the same order of magnitude as the mutual distance between the centers of two subunits. As a consequence, when this distance is large, the largest effect is bound to occur in the visible (or in the infrared),

while when this distance is comparatively smaller, it occurs in the ultraviolet.

The present results, together with the results of our previous work (Saija et al. 2001), suggest that both grain aggregates with a quite low degree of clustering and equivalent-mass homogeneous spheres exhibit larger extinction cross sections per unit mass in the visible than aggregates with a large number of basic constituents. This behavior has two major implications: the first pertains to the modeling procedure, and the second is related to the dust-mass balance in the interstellar medium.

The implication for the dust-mass balance may be relevant since the visible part of the extinction curve is mainly produced by the large component of the dust-mass spectrum. Significantly, aggregates composed of a comparatively small number of large monomers are suitable candidates for explaining interstellar polarization (Wurm & Schnaiter 2002).

REFERENCES

Abramowitz, M., & Stegun, I. A. 1965, Handbook of Mathematical Functions (New York: Dover)
Borghese, F., Denti, P., & Saija, R. 1994, Appl. Opt., 33, 484
———. 2002, Scattering from Model Nonspherical Particles (London: Springer)
Borghese, F., Denti, P., Saija, R., Iatì, M. A., & Sindoni, O. I. 2001, J. Quant. Spectrosc. Radiat. Transfer, 70, 237
Borghese, F., Denti, P., Saija, R., Toscano, G., & Sindoni, O. I. 1984, Aerosol Sci. Tech., 3, 227
Borghese, F., Denti, P., Toscano, G., & Sindoni, O. I. 1980, J. Math. Phys., 21, 2754
Bradley, J. P., et al. 1999, Science, 285, 1716
Chokshi, A., Tielens, A. G. G. M., & Hollenbach, D. 1993, ApJ, 407, 806
Chylek, P., Videen, G., Geldart, D. J. W., Dobbie, J. S., & Tso, H. C. W. 2000, in Light Scattering by Nonspherical Particles, ed. M. I. Mishchenko, J. W. Hovenier, & L. D. Travis (San Diego: Academic Press), 274
Dominik, C., & Tielens, A. G. G. M. 1995, Philos. Mag. A, 72, 783
———. 1996, Philos. Mag. A, 73, 1279
Draine, B. T. 1985a, Protostars and Planets II, ed. D. C. Black & M. S. Matthews (Tucson: Univ. Arizona Press), 621
———. 1985b, ApJS, 57, 587
———. 1988, ApJ, 333, 848
Fucile, E., Borghese, F., Denti, P., Saija, R., & Sindoni, O. I. 1997, IEEE Trans. Antennas Propagation, 45, 868
Gérardy, J. M., & Ausloos, M. 1982, Phys. Rev. B, 25, 4204
Hagen, J. I., & Greenberg, J. M. 1990, ApJ, 361, 251
Jackson, D. J. 1975, Classical Electrodynamics (New York: Wiley)
Jura, M. 1980, ApJ, 235, 63
Krueger, F. R., & Kissel, J. 1989, Origins Life Evol. Biosphere, 19, 87
Mathis, J. S. 1996, ApJ, 472, 643
Mathis J. S., & Whiffen, G. 1989, ApJ, 341, 808
Michel, B., Henning, Th., Stognienko, R., & Rouleau, F. 1996, ApJ, 468, 834
Mishchenko, M. I., & Mackowski, D. W. 1996, J. Quant. Spectrosc. Radiat. Transfer, 55, 683
Mukai, T., Ishimoto, H., Kozasa, T., Blum, J., & Greenberg, J. M. 1992, A&A, 262, 315
Ossenkopf, V. 1993, A&A, 280, 617
Purcell, E. M., & Pennypacker, C. R. 1973, ApJ, 186, 705
Quinten, M., Kreibig, U., Henning, Th., & Mutschke, H. 2002, Appl. Opt., 41, 7102
Rouleau, F., & Martin, P. G. 1991, ApJ, 377, 526
Saija, R., Iatì, M. A., Borghese, F., Denti, P., Aiello, S., & Cecchi-Pestellini, C. 2001, ApJ, 559, 993
Saija, R., Iatì, M. A., Denti, P., Borghese, F., Giusto, A., & Sindoni, O. I. 2003, Appl. Opt., 42, 2785
Stratton, J. A. 1941, Electromagnetic Theory (New York: McGraw-Hill)
Suh, K.-W. 1999, MNRAS, 304, 389
———. 2000, MNRAS, 315, 740
Vaidya, D. B., Gupta, R., Dobbie, J. S., & Chylek, P. 2001, A&A, 375, 584
Waterman, P. C. 1971, Phys. Rev. D, 3, 825
Weidenschilling, S. J., & Ruzmaikina, T. V. 1994, ApJ, 430, 713
Wiscombe, W. J. 1979, Mie Scattering Calculations: Advances in Technique and Fast, Vector-shaped Computer Codes (Internal Rep.; Boulder: NCAR)
Wolff, M. J., Clayton, G. C., & Gibson, S. J. 1998, ApJ, 503, 815
Wolff, M. J., Clayton, G. C., Martin, P. G., & Sculte-Ladback, R. E. 1994, ApJ, 423, 412
Wurm, G., & Schnaiter, M. 2002, ApJ, 567, 370